Advances in Water Resources 107 (2017) 147–159

Contents lists available at ScienceDirect

Advances in Water Resources

journal homepage: www.elsevier.com/locate/advwatres

# Catchment tomography - An approach for spatial parameter estimation

D. Baatz[a,b,*], W. Kurtz[a,b], H.J. Hendricks Franssen[a,b], H. Vereecken[a,b], S.J. Kollet[a,b]

[a] Forschungszentrum Jülich GmbH, Institute of Bio- and Geosciences, IBG-3 (Agrosphere), Germany
[b] Centre for High-Performance Scientific Computing in Terrestrial Systems (HPSC-TerrSys), Geoverbund ABC/J, Jülich, Germany

ARTICLE INFO

*Article history:*
Received 1 July 2016
Revised 30 May 2017
Accepted 11 June 2017
Available online 16 June 2017

*Keywords:*
Distributed hydrological modelling
Data assimilation
Radar rainfall estimates
Parameter estimation
Joint state-parameter update
Tomography

ABSTRACT

The use of distributed-physically based hydrological models is often hampered by the lack of information on key parameters and their spatial distribution and temporal dynamics. Typically, the estimation of parameter values is impeded by the lack of sufficient observations leading to mathematically underdetermined estimation problems and thus non-uniqueness. Catchment tomography (CT) presents a method to estimate spatially distributed model parameters by resolving the integrated signal of stream runoff in response to precipitation. Basically CT exploits the information content generated by a distributed precipitation signal both in time and space. In a moving transmitter-receiver concept, high resolution, radar based precipitation data are applied with a distributed surface runoff model. Synthetic stream water level observations, serving as receivers, are assimilated with an Ensemble Kalman Filter. With a joint state-parameter update the spatially distributed Manning's roughness coefficient, *n*, is estimated using the coupled Terrestrial Systems Modelling Platform and the Parallel Data Assimilation Framework (TerrSysMP-PDAF). The sequential data assimilation in combination with the distributed precipitation continuously integrates new information into the model, thus, increasingly constraining the parameter space. With this large amount of data included for the parameter estimation, CT reduces the problem of underdetermined model parameters. The initially biased Manning's coefficients spatially distributed in two and four fixed parameter zones are estimated with errors of less than 3% and 17%, respectively, with only 64 model realizations. It is shown that the distributed precipitation is of major importance for this approach.



## 1. Introduction

Hydrological models support decision making for hydropower generation and water resources management, such as irrigation scheduling and drinking water supply (Paiva et al., 2013). They are powerful tools for predicting extreme events and designing flood control measures (Pauwels and De Lannoy, 2009; Shi et al., 2014). Uncertainties in model structure, forcings and parameters are still challenging issues limiting the forecast reliability (Reichle, 2008; Liu et al., 2012; Rakovec et al., 2012; McMillan et al., 2013; Shi et al., 2014). Sophisticated, distributed hydrological models have been developed in the last decades. The number of uncertain model parameters is large for these models (Pokhrel and Gupta, 2011; Shi et al., 2014), which makes parameter estimation a difficult task. The number of unknown parameters is usually larger than the number of observations (Yeh, 1986; Bourdin et al., 2012), resulting in an underdetermined parameter identification problem i.e. several different parameter sets may result in the same model accuracy, which is referred to as non-uniqueness.

For the calibration of hydrological models, stream water level or discharge are often the main variables to be conditioned on. For flood forecasting, which is, besides the research on hydrological processes, one of the main purposes of hydrological models (Moradkhani et al., 2005), discharge is one of the most important output variables. Discharge is influenced by practically all model states and parameters. As response to precipitation, surface runoff and stream discharge are formed along different paths and time scales, depending on the precipitation pattern and upstream parameters. Therefore, discharge constitutes an integrated response signal comprising information on e.g. upstream parameters, topography, system states, and precipitation.

This study presents a catchment tomography (CT) approach for resolving the aforementioned integrated response signals with data assimilation techniques. Conceptually, precipitation, which is highly variable in time and space, serves as moving transmitter; and several stream gauges, measuring the generated streamflow

* Corresponding author.
*E-mail address:* d.baatz@fz-juelich.de (D. Baatz).

http://dx.doi.org/10.1016/j.advwatres.2017.06.006

at different locations within the catchment, serve as receivers. In the CT, stream water level observations are assimilated into a distributed hydrological model, which is forced with high resolution, radar based precipitation data. In a joint state-parameter update with the Ensemble Kalman Filter (EnKF), spatially distributed flow parameters are updated together with the stream water level. The sequential assimilation of stream water level continuously integrates new information into the hydrological model with every precipitation event. This large amount of information used for parameter estimation permits the mitigation of non-uniqueness problems. Section 2 gives a review on data assimilation methods and an explanation of the proposed catchment tomography approach. The experimental set-up, the sample catchment, the model and the data assimilation framework are introduced in Section 3. Section 4 presents the results of the different experiments and conclusions are drawn in the final Section 5.

## 2. Theory and background

### 2.1. Data assimilation

In recent years, an increasing amount of data has been made available in the geosciences via the analysis of subsurface, land surface and atmospheric processes, due to an enhanced application of remote sensing and in-situ measurement techniques (McLaughlin, 2002; Reichle, 2008; Montzka et al., 2012). These data enable the application of advanced, data-intensive methods and may lead to new approaches of data assimilation mitigating the problems of underdetermined models and associated large uncertainties of estimated states and parameters. Data assimilation comprises several techniques for merging multisource data, downscaling, reduction of data volumes and inter- or extrapolation of distributed data (Reichle, 2008). The aim of data assimilation is to reduce uncertainty by combining data of different sources. Often, observational data are integrated into models to gain a new estimate with lower uncertainty than both the observation and the model result alone (Reichle, 2008). Variational data assimilation methods optimize model states on the basis of complete time series of observations, by assimilating measurement data in batch while sequential data assimilation continuously integrates newly available data in a sequential fashion (Liu and Gupta, 2007; Reichle, 2008; Rakovec et al., 2015).

The Kalman Filter (Kalman, 1960) and its extensions are sequential methods which are widely used (Evensen, 1994; Burgers et al., 1998; Reichle et al., 2002b). The model forecast of a state or a parameter value is updated with observations using the Kalman gain, a weighting factor relating model and measurement uncertainties. The traditional Kalman Filter assumes the model system to be linear and the probability density distribution of the states to be Gaussian (Kalman, 1960; McLaughlin, 2002; Reichle, 2008). This assumption is unrealistic for most hydrologic applications. The Extended Kalman Filter linearizes the estimation of the model covariances, which often results in an unbounded growth of the error covariance and involves high computation costs (McLaughlin, 2002). The Ensemble Kalman Filter (EnKF) (Evensen, 1994; Burgers et al., 1998) is more robust under conditions of non-linearity and non-Gaussianity and is a commonly applied alternative. The model error covariance needed for the update step is estimated from an ensemble of possible model states and does therefore not need to be propagated forward in time explicitly. That reduces the computational burden and does not assume a Gaussian distribution of model states. Nevertheless, the performance of EnKF is only optimal if uncertain states (and parameters) are Gaussian.

The EnKF is a stochastic filter because observations are perturbed to avoid an underestimation of the analysis error covariance (Burgers et al., 1998). Whitaker and Hamill (2002) argue that the random perturbation adds additional sampling error, especially for small ensembles and thus propose a deterministic Ensemble Square Root Filter which does not need perturbed observations. Further deterministic approaches for Ensemble Kalman Filters are proposed by Anderson (2001) and Bishop et al., (2001) and reviewed by Tippett et al. (2003).

A fundamental problem of approximating the error covariance by an ensemble of simulations is the limited ensemble size, which for several reasons leads to a systematic underestimation of the ensemble variance. In turn, the underestimation of model variance results in assigning too large weights to the model and too small weights to the measurements, and can ultimately result in small weights for the measurements such that the model simulation results experience no improvement by the incorporation of the data. This is also called filter divergence (van Leeuwen, 1999; Ehrendorfer, 2007; Franssen and Kinzelbach, 2008). Houtekamer and Mitchell (1998) saw a main reason for the decreasing ensemble spread in an inbreeding of the ensemble: the background error statistics needed for determining the Kalman gain are calculated from the same ensemble which is then updated. For this reason, an underestimation in ensemble error covariance is sometimes referred to as filter inbreeding in literature. van Leeuwen (1999) pointed out that the inbreeding is only part of the problem. The approximated forecast error covariance includes inaccuracies, because of sampling errors, especially for small ensemble sizes. Due to nonlinearities in the update step these inaccuracies lead to an underestimation of the analysis error covariance.

Observations are not always available at regular time intervals or at times the model is updated. Therefore, methods were developed to allow for assimilating observations made between the last updating time step and the current time step. This is generally referred to as asynchronous or four dimensional variational data assimilation (Sakov et al., 2010; Rakovec et al., 2015). A common example is the Ensemble Smoother (Evensen and van Leeuwen, 2000) which considers observations made within a specified time interval.

#### 2.1.1. Data assimilation in hydrology

Early work on data assimilation in hydrology was in the 1980ś (Kitanidis and Bras, 1980b; Kitanidis and Bras, 1980a) with the extended Kalman Filter and it was shown in these works that streamflow forecasts could be improved by integrating real-time observations of uncertain precipitation and discharge observations into a conceptual hydrological model. Sequential data assimilation was not applied very frequently in the 1980 s and 1990 s, related most probably to the earlier indicated limitations of the classical and extended Kalman filter. Data assimilation has increasingly been applied in the area of water resources in the past two decades (Clark et al., 2008; Reichle, 2008; Rakovec et al., 2012; Reichle et al., 2002a). A comprehensive review on data assimilation in terrestrial systems is given by Montzka et al. (2012). Madsen et al. (2003) assimilated stream water levels into a distributed hydrological model. They showed improvements in the model forecast by assimilating water levels and fluxes into MIKE 11. Pauwels and De Lannoy (2006) performed synthetic experiments with a retrospective EnKF and mitigated the effect of a bias in the model's initial conditions by assimilating discharge. Furthermore they showed that a bias in soil moisture resulting from strongly biased precipitation input can be reduced by assimilating discharge. Clark et al. (2008) updated hourly distributed model states (soil moisture, aquifer storage and surface storage) by assimilating four streamflow observations with the EnKF or Ensemble Square Root Filter. McMillan et al. (2013) updated the same states but considered the time lag between downstream gauging information and upstream model states by applying a recursive ensemble Kalman

Filter on their operational system. Rakovec et al. (2012) examined different experimental designs in synthetic and real-world studies and showed that the number of observation locations has a more significant impact on the data assimilation than a frequent update. This confirmed findings by Clark et al. (2008) that distributed observations are essential for updating distributed states. Camporese et al. (2009b) and Bailey and Bau (2012) both assimilated pressure head and streamflow in the surface-subsurface flow model CATHY. Their synthetic experiments on an idealized v-catchment showed that the assimilation of the pressure head is much more successful in improving streamflow and pressure head estimations than the streamflow assimilation. The same was shown by Camporese et al. (2009a) for a distributed catchment model. The experiments by Camporese et al. (2009b) even showed that the assimilation of streamflow alone had a negative impact on the simulated subsurface states compared to open loop simulations. The reason for this might be that, for both studies Camporese et al. (2009a) and Camporese et al. (2009b) assimilated stream flow at only one single observation location at the catchment outlet.

#### 2.1.2. Parameter estimation with data assimilation

While data assimilation is usually applied for optimizing model states, it can also be used for estimating or improving model parameters (Annan et al., 2005; Franssen and Kinzelbach, 2008). Using data assimilation techniques for parameter estimation offers, in contrast to the usual batch calibration, the advantage of accounting for parameter uncertainty and time-variant parameters (Moradkhani et al., 2005). Furthermore, the model parameterization is continuously improved and not limited to past observations. Moradkhani et al. (2005) presented a method for combining state and parameter estimation by a dual EnKF. Vrugt et al. (2005) simultaneously performed data assimilation and parameter estimation by combining the state update with an external parameter optimization. This approach was successfully applied by Vrugt et al. (2006) for operational stream flow forecasting. A common technique for a joint state-parameter estimation is the augmentation of the state vector with the parameters to be updated (Chen and Zhang, 2006; Franssen and Kinzelbach, 2008; Kurtz et al., 2012). The covariances between the unknown parameters and the model states at observation locations are included into the state covariance matrices, yielding an augmented state-parameter covariance matrix.

Parameter estimation for hydrological and hydraulic models by data assimilation techniques has been investigated in several studies. Moradkhani et al. (2005) updated five model parameters in a conceptual model together with streamflow using a dual state-parameter estimation approach. Franssen and Kinzelbach (2008) made a comprehensive study on the impact of ensemble size, number of observations and observation frequency for synthetic data assimilation with different variants of the EnKF and with and without joint parameter estimation. They found that joint state-parameter estimation significantly increases filter inbreeding. This could be mitigated by introducing a damping factor, which diminishes the update. Kurtz et al. (2012) assimilated hydraulic head data for a stream-aquifer flow problem and jointly estimated time variant riverbed hydraulic conductivities. By applying covariance inflation, a more efficient parameter estimation was achieved. Ground water head and stream discharge observations were assimilated with and without parameter update by Rasmussen et al. (2015). The authors showed that a large ensemble size or localization methods are beneficial for parameter updates in a coupled surface - subsurface model. (Pathiraja et al., 2016) updated time variant parameters after deforestation events with a locally linear EnKF and thereby improved stream flow predictions.

### 2.2. Catchment tomography

Tomography maps an object's physical properties by inverting a signal that has been transmitted through many different cross sections. This imaging technique is already applied in groundwater hydrology for determining aquifer properties by series of pumping tests, called hydraulic tomography. By measuring changes in hydraulic head in response to various pumping tests performed at different wells, spatially distributed information on the aquifer response is gained and inverted to estimate the hydraulic properties of interest (Yeh and Liu, 2000; Li et al., 2007).

With the aim of distributed parameter estimation, this study applies the tomographic concept on a hydrological catchment. Instead of pumping water, the natural precipitation, which is monitored in high resolution by radars, is used as a transmitter. Stream gauges are the receivers measuring water levels as the catchment responds to precipitation water input and upstream flow parameters. These measurements are inverted for estimating distributed model hydraulic parameters.

The inversion is done by joint state-parameter estimation with the EnKF using the state-augmentation approach. Stream water level observations at multiple locations are assimilated into the distributed model. The data assimilation allows for accounting for the changing uncertainty of model parameters and model forcings during the inversion process. A further advantage of using this data assimilation method instead of classical calibration is the sequential and efficient integration of newly available information into the model. This way a large amount of data can be processed and utilized for the parameter estimation, which reduces the non-uniqueness problem of parameter estimation. Note that, parameter uncertainty in an inverse framework is controlled by uncertain model input and model structural errors. This uncertainty will remain in any case, thus, there cannot be a unique solution to the parameter identification problem.

Every precipitation event initiates a new, different hydrological response of the catchment. If there is rain in only a small part of the study area, the resulting streamflow is especially meaningful for this region. Therefore the application of distributed and accurate precipitation forcing on the hydrological model is a key driver for this parameter estimation method. Temporal and spatial resolution need to be high enough to enable the model to simulate spatially distributed runoff generation at relevant hydrological time scales. The temporal variability of precipitation leads to changes in stream water level with time. This fluctuating stream water level as response to temporally variable precipitation is the essential signal to invert for the temporally constant model parameters.

In this study, the proposed approach was assessed by estimating the Manning's roughness coefficient, $n$. For a synthetic surface runoff model with real precipitation input several experimental set ups are evaluated. Because the model does not consider subsurface flow, simulated streamflow is sensitive to the Manning's coefficient.

While several studies have assimilated stream water level into hydrological models to update states and, in many cases, also model parameters, catchment tomography presents an approach that combines high frequency stream water level assimilation with high resolution precipitation data based on rain radar transmitter information. We hypothesize that the large amount of data which is continuously and efficiently integrated into the model by sequential data assimilation permits the mitigation of the non-uniqueness problem in distributed hydraulic parameter estimation.

## 3. Methodology

Synthetic experiments were performed using the hydrologic component of the Terrestrial Systems Modeling Platform

(TerrSysMP, Shresta et al., 2014;) with integrated parallel data assimilation technology (TerrSysMP-PDAF; Kurtz et al., 2016) to verify catchment tomography for parameter estimation and to test the efficiency of the approach under different experimental set-ups. For testing purposes, synthetic models are of advantage, because structural model and systematic measurement errors are known, which allows for investigating the suitability of the methodology in principle. Furthermore, synthetic experiments are a useful technique to examine possible experimental designs (Pokhrel and Gupta, 2011) and identify potential obstacles.

We simulated surface runoff in a two-dimensional domain of varying topography and by excluding subsurface and atmospheric processes. The modelling domain has horizontal dimensions of $72 \times 72$ rectangular grid cells of size $500 \times 500$ m and one vertical layer. The surface permeability is set to zero to simulate surface runoff only. Precipitation is introduced as upper boundary condition. In this 2D set-up, the surface runoff was influenced solely by the friction slope $S_f$ (-) and Manning's roughness coefficient $n$ ($TL^{-1/3}$) based on the Manning's Eq. (1). The relationship is described by the Manning's equation (Chow et al., 1988; Kollet and Maxwell, 2006)

$$v = \frac{\sqrt{s_f}}{n} \psi_s^{\frac{2}{3}} \tag{1}$$

with $v$ being the flow velocity ($LT^{-1}$), and $\psi_s$ the surface ponding depth (L).

At the horizontal boundaries there is no inflow but only outflow $q_{\text{out}}$ out of the modelling domain with a gradient boundary condition specified in Eq. 2:

$$q_{\text{out}} = \frac{\sqrt{s_{\text{f,outlet}}}}{n_{\text{outlet}}} \psi_{s,\text{outlet}}^{\frac{3}{5}} \tag{2}$$

The slope was derived from a digital elevation model and $n$ was the only parameter to be estimated. The Manning's coefficient $n$ is an empirical parameter describing the roughness of a surface, which influences the flow velocity.

Because there is no subsurface in this simplified scenario, rivers would dry out in periods without precipitation due to the absence of base flow. In order to avoid this, an average runoff was simulated by including an additional steady state background flux equalling an average baseflow rate of 500 mm per year. This was integrated in the model as the top boundary condition and was constant in time and space.

This background flux was also used for forcing the spin-ups, which were performed without distributed precipitation. Spin-ups started with an initial water level of zero and were run until steady state was achieved. To account for all possible transient scenarios the spin-ups lasted 10 days (2880 time steps). The time of concentration of the model is relatively short due to nonexistence of subsurface storage. The steady state water level fields resulting from the spin-up served as initial conditions for the simulations.

### 3.1. The ensemble Kalman filter for joint state and parameter estimation

The Manning's coefficient $n$ was updated by assimilating water level observations with a joint state-parameter update with the EnKF with a state-augmentation approach. The state vector of the ensemble Kalman filter is therefore augmented by a parameter vector. Thus, parameters are updated jointly by state observations only, via the covariances between the parameter ensemble and the ensemble of state forecasts at the observation locations. For the parameter update, the Manning's $n$ was $\log_{10}$-transformed. Please refer to the Appendix for a detailed explanation of the filter including equations.

Both water level and $n$ were updated hourly with an ensemble of 64 members. A more frequent update is theoretically possible, because stream water level observations are available at every model time step. However, the impact of spurious correlations on state and parameter updating is enhanced by frequent updating, especially if parameters are updated simultaneously. Preliminary experiments showed that an updating interval of one hour is a good trade-off for not missing significant peak flows induced by the applied precipitation time series.

### 3.2. TerrSysMP – PDAF

The Terrestrial Systems Modelling Platform (TerrSysMP) (Shrestha et al., 2014), a coupled biogeophysical earth system model, is used in this study. TerrSysMP consists of the numerical weather prediction model COSMO-DE (Baldauf et al., 2011), which is the operational model of the German Weather Service, the NCAR Community Land Model 3.5 (CLM) (Oleson et al., 2008) and the hydrologic surface and subsurface flow model ParFlow (Ashby and Falgout, 1996; Jones and Woodward, 2001; Kollet and Maxwell, 2006). These three independently developed component models are coupled via the external Ocean Atmosphere Sea Ice Soil coupler (OASIS3) (Valcke, 2013). In addition to running the fully coupled system, it is possible to run any of the three component models independently within TerrSysMP.

In this study, ParFlow is applied stand-alone based on the modular approach of TerrSysMP. ParFlow is a 3D variably-saturated subsurface and overland flow model. It is based on the 3D Richards equation and able to simulate heterogeneous parameter distributions with high resolution (Maxwell et al., 2010). ParFlow shows excellent parallel efficiency and therefore allows for high-resolution large-scale hydrologic simulations as shown by Kollet et al. (2010) and Maxwell et al. (2015).

An overland flow boundary condition simulator allows simulation of surface flow based on the shallow water equation (Kollet and Maxwell, 2006). The continuity equation for shallow overland flow in two dimensions is given by

$$\frac{\delta \psi_s}{\delta t} = \nabla \times (v \psi_s) + q_r(x) \tag{3}$$

with $\psi s$ being the surface ponding depth [L], $t$ the time [T], $v$ the vertically averaged flow velocity [L/T], $q_r(x)$ the rainfall rate. The relationship between flow depth and discharge is given by Manning's Eq. (1).

The overland flow model is solved with a Newton-Krylov method (Jones and Woodward, 2001; Kollet and Maxwell, 2006) and discretized spatially by a standard upwind finite control volume scheme and temporally by an implicit backward Euler scheme (Kollet and Maxwell, 2006). Eq. 3 is integrated into the Richards equation as a free surface overland flow boundary condition. In this work, only overland flow is simulated in a single vertical layer by setting the permeability and therefore the exchange with the subsurface to zero.

TerrSysMP has recently been coupled to the Parallel Data Assimilation Framework (PDAF) (Nerger et al., 2005; Nerger and Hiller, 2013) by Kurtz et al., (2016). PDAF is a parallelized data assimilation system, which can be combined with a numerical model to allow for efficient ensemble data assimilation. PDAF parallelizes not only the forward ensemble simulations but also the analysis step to provide a fully parallelized framework for data assimilation. A large number of different filter methods are available for this purpose.

Kurtz et al. (2016) implemented a joint state-parameter update with TerrSysMP-PDAF to estimate spatially distributed fields of the Manning's roughness parameter or saturated hydraulic conductivities. An important feature is the exchange of the relevant

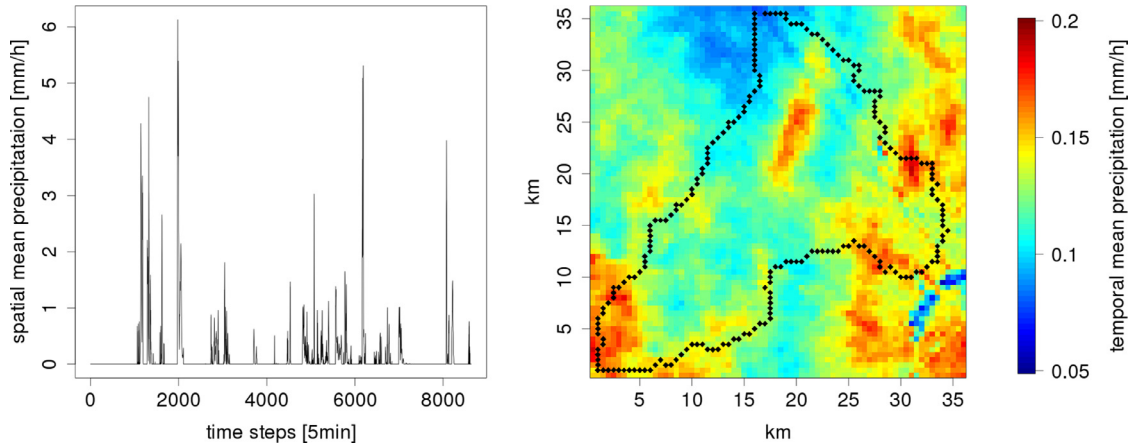


**Fig. 1.** Time series of spatial mean precipitation (left) and spatially distributed temporal mean precipitation (right) for the study period. The Upper Erft – Swist Catchment is marked in the model domain.

states and fluxes between the ensemble and filter in memory. Thus, no IO is required, which affords the application of the system to very large problem sizes. For details on the implementation of TerrSysMP-PDAF the reader is referred to Kurtz et al. (2016).

### 3.3. Synthetic 2D experiments

#### 3.3.1. Sample catchment and data

As aforementioned, the catchment tomography approach was applied to a synthetic catchment mimicking the Swist and Upper Erft catchments in Western Germany discharging into the Rhine River. The catchment was selected, because of the availability of high resolution radar precipitation data, several stream gauges within the catchment and its proneness to flooding due to local convective precipitation events. Topography and distributed precipitation were obtained from real data. For the synthetic experiments, synthetic stream gauge water level observations modelled in the reference run at the locations of real stream gauges were used.

The Swist and Upper Erft catchments are located in the Eifel Mountains southwest of Bonn (Germany) between 50.45°N and 50.80°N and 6.56°E and 7.11°E. The catchment area is about 530km² and elevation ranges from 72 to 573 m.a.s.l. The rectangular domain spanning the watershed is $36 \times 36$ km wide with a spatial resolution of 500 m. The resulting model domain of $72 \times 72$ cells is convenient to parallelize using regular domain decomposition. Within the area there are a few small towns and villages, many of them situated nearby rivers and channels.

#### 3.3.2. Precipitation from rain radar

The model was forced with high resolution radar precipitation data from the polarimetric X-Band Doppler radar BoXPol of the Meteorological Institute, Bonn University (Germany). More details on the radar can be found in Diederich et al. (2015a) and Diederich et al. (2015b). The rain rate was estimated from radar reflectivity for rain rates larger than 8 mm/h and from specific phase shift for rain rates smaller than 8 mm/h. The spatial and temporal resolution of the precipitation fields are 500 m and 5 minutes, respectively. In the experiments presented here, a 30-day time series of June 2011 was applied. Fig. 1 shows the spatial and temporal mean precipitation for the study period and area. The spatial average total precipitation for the 30 days is 87.81 mm. The high resolution precipitation forcing is expected to be the main driver of the proposed parameter estimation system.

Experiments were first performed with error-free precipitation. Identical precipitation fields, as estimated from the rain radar, were applied to the reference simulation and all realizations. The same experiments were then performed with an ensemble of perturbed precipitation data to account for radar error. To generate the ensemble, precipitation was perturbed by a multiplicative, spatially and temporally correlated error. It was assumed that the correlation length of the precipitation error is similar to the correlation length of the precipitation itself. From precipitation data we estimated a temporal correlation length of 1 h and a spatial correlation length of 8 km. For avoiding negative error values the multiplicative error was chosen to be lognormally distributed with a mean of 1 and a standard deviation of 0.5. To generated this data, first 3D correlated, normally distributed data fields with mean 0.1115718 and standard deviation 0.4723807 were generated with a geostatistical simulation program from the geostatistical software package gstat (R) (Pebesma, 2004; R Development Core Team, 2008). These fields were then transformed to lognormally distributed error fields which by the transformation got the desired mean of 1 and standard deviation of 0.5.

#### 3.3.3. Stream water level observation locations and observation error

There are 15 real-world stream gauges in the model domain comprising the Upper Erft and Swist catchments that are operated by LANUV NRW (State Department for the Environment, Nature and Consumerism of North Rhine-Westphalia) and the Erft-Verband (Erft Natural Resources District). The latter supplied the geographical information of the different gauges. Nine stream gauges are located in the Erft river and its tributaries, two in the Swist river and four in the Rotbach. The Rotbach is actually not part of the Upper-Erft and Swist catchments, as it discharges into the Lower-Erft just north of the study area, but the four gauges are located in the computational model domain and are therefore included in the experiments. For the synthetic studies, the locations of the 15 gauges were used as synthetic observation points. The locations of stream gauges (Fig. 2) were assigned to the equivalent grid cells in the model. Due to the resolution of 500 m and the involved approximations, the locations of some of the gauges needed to be corrected to be located in the river grid cells. Streams are not explicitly modeled in ParFlow but are formed by runoff generation. Thus, the spatial scale of water levels is 500 m which is larger than most rivers. If real instead of synthetic stream water level or discharge measurements are assimilated, a measurement operator needs to be applied to consider the scale mismatch between measurement and model.

The discharge measurement error is usually a function of the flow rate (Di Baldassarre and Montanari, 2009) and may differ con-

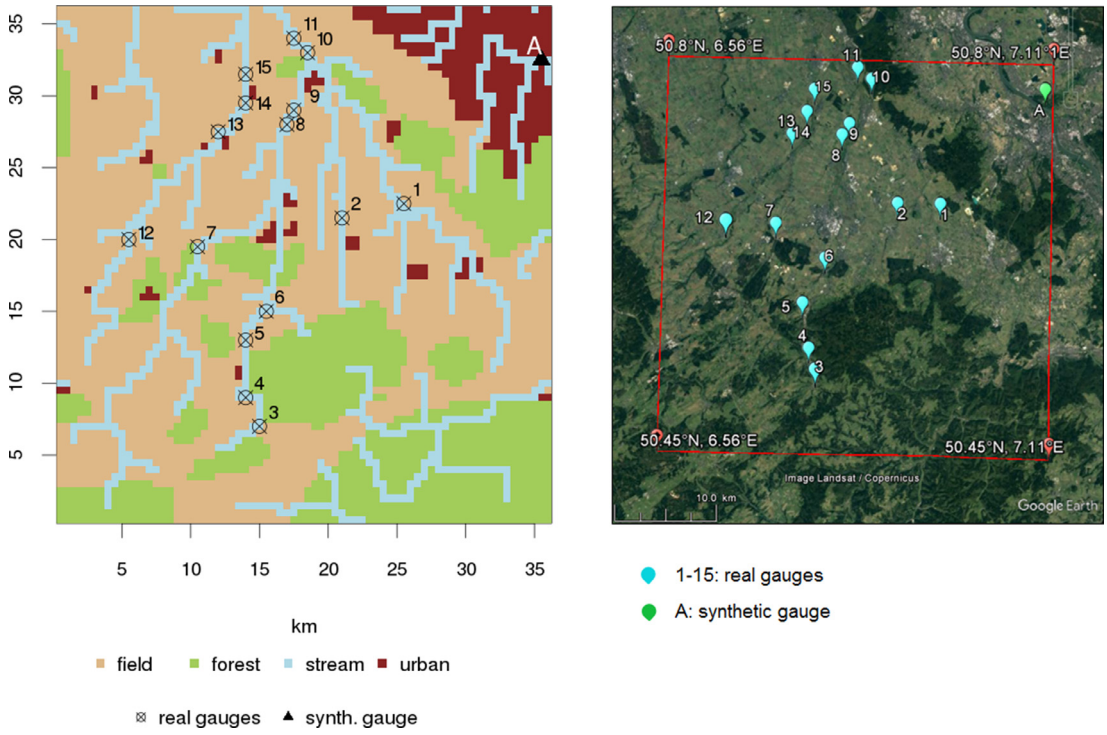


**Fig. 2.** Locations of stream water gauges and the four $n$ parameter zones of the study domain (left). The urban, field and forest zones are comprised in the zone hillslopes for the scenarios with only two zones of $n$. (right) Google Earth Landsat image to derive land use based zonation.

siderably between different gauges (Tilo Keller, Erftverband, Germany, personal communication, April 24th 2015).

Observations were perturbed with a random error drawn from a normal distribution with zero mean. Two different implementations for the standard deviation of the error were tested: An absolute observation error with a standard deviation constant in time and space, and a relative observation error depending on the water level. The absolute error was drawn from a distribution with a standard deviation equal to 30% of the mean water level at all observation points at steady state, with the constant background flux but without distributed precipitation. The relative observation error in contrast has a standard deviation of 50% of the synthetically observed water level at the specific stream gauges and observation times. For the case of an absolute observation error, the relative errors of the individual stream gauges differed considerably and are smaller for peak than for low flow conditions. Thus, by applying an absolute observation error, headwater gauges generally have a larger observation error than by applying a relative error, because the water level is lower in upstream areas. This results in a reduced update for these areas if the absolute error is applied. The relative observation error is, on average, larger than the absolute observation error by a factor of about three.

### 3.4. Simulation set-up

#### 3.4.1. Scenarios and implementations of precipitation and observation error

Because stream water level was assimilated, observations were only available within streams. The challenge of this set-up was to estimate the water level and Manning's $n$ outside the streams, where no measurements were available. Two different scenarios of parameter heterogeneity were applied in combination with different implementations of precipitation forcing and observation error.

For scenario A (SA), the model domain was divided into two discrete, discontinuous zones representing the streams and hillslopes with different $n$. The zones were assigned according to the stream segmentation derived from the DEM with GRASS GIS. For scenario B (SB), the zone "hillslopes" from SA was additionally divided into the zones urban, field and forest according to land use in the sample catchment estimated from Google Earth Landsat images. The distribution of these zones and the corresponding Google Earth map are shown in Fig. 2.

For scenario SA and SB, different cases of observation errors were considered. In the first case (c1), experiments were performed with error-free precipitation and an absolute observation error (as explained in Sections 3.3.2 and 3.3.3). In a second case (c2) a relative observation error was used in combination with error-free precipitation. The third case (c3) combines the relative observation error and perturbed precipitation forcing and is therefore the most realistic one. To evaluate the need for spatially distributed precipitation data for the proposed catchment tomography approach, a fourth case (c4) was added. For c4, spatially averaged, homogeneous precipitation fields were applied to the model realizations SA and SB. These fields were generated by computing the spatial mean precipitation for every time step and realization of precipitation fields. This spatial average was then applied to every single grid cell.

All experiments of an individual land cover scenario (SA and SB) are updated with synthetic observations from the same reference $n$. Every experiment was performed with 64 realizations. Table 1 gives an overview of the experiments.

#### 3.4.2. Parameterization and ensemble generation

The uncertainty of the empirical $n$ is large and literature values differ considerably. In order to use realistic values for the synthetic experiments, Manning's coefficients $n$ suggested in Karnahl (2008), Chow et al., (1988), Arcement and Schneider (1989) and Pasche et al. (2006) were considered for the land use and stream characteristics in the Swist and Upper Erft watersheds. Manning's reference values for the different zones of SA and SB are summarized in Table 2. The spatial distribution of $n$ fields of the individual ensemble members had the same areal zonation as the

**Table 1**
Overview of data assimilation experiments. SA and SB are the different scenarios A and B with 2 and 4 parameter zones, respectively. c1 – c4 are the four cases explained above.

| Exp. name | # Parameter zones | Precipitation | Observation error | Gauges |
|---|---|---|---|---|
| With absolute observation error and error-free precipitation | | | | |
| SA-c1 | 2 | error-free | absolute error | real |
| SB1-c1 | 4 | error-free | absolute error | real |
| SB1-c1+S1 | 4 | error-free | absolute error | real+S1 |
| SB2-c1 | 4 | error-free | absolute error | real |
| With variable observation error and error-free precipitation | | | | |
| SA-c2 | 2 | error-free | 50% | real |
| SB1-c2 | 4 | error-free | 50% | real |
| SB1-c2+S1 | 4 | error-free | 50% | real+S1 |
| SB2-c2 | 4 | error-free | 50% | real |
| With variable observation error and perturbed precipitation | | | | |
| SA-c3 | 2 | perturbed | 50% | real |
| SB1-c3 | 4 | perturbed | 50% | real |
| SB1-c3+S1 | 4 | perturbed | 50% | real+S1 |
| SB2-c3 | 4 | perturbed | 50% | real |
| With variable observation error, spatially homogeneous perturbed precipitation | | | | |
| SB1-c4 | 4 | perturbed, spat. homogeneous | 50% | real |
| SB2-c4 | 4 | perturbed, spat. homogeneous | 50% | real |

**Table 2**
Reference and initial guess Manning's values.

| Scenario | Zone | Reference $n$ | Lognormal distribution to draw initial $n$ | |
|---|---|---|---|---|
| | | [min/m$^{1/3}$] | Median [min/m$^{1/3}$] | Log standard deviation [min/m$^{1/3}$] |
| SA | streams | 0.0004 | 0.0020 | 2 |
| | hillslopes | 0.0020 | 0.0004 | 2 |
| SB1 | streams | 0.0007 | 0.0010 | 1 |
| | urban | 0.0003 | 0.0010 | 1 |
| | fields | 0.0010 | 0.0010 | 1 |
| | forest | 0.0040 | 0.0020 | 1 |
| SB2 | streams | 0.0007 | 0.0010 | 2 |
| | urban | 0.0003 | 0.0010 | 2 |
| | fields | 0.0010 | 0.0010 | 2 |
| | forest | 0.0040 | 0.0020 | 2 |

respective reference fields, i.e. it was assumed that the zonation is known from e.g. satellite information. The $n$ values were homogeneous within each zone, but parameters of individual zones were perturbed independently from each other. They were drawn from lognormal distributions, as specified in Table 2. SB consists of two experiments with different spreads in the initial $n$. SB1 has an initial parameter spread of standard deviation 1 and SB2 of standard deviation 2. Note, that the major part of the urban zone of SB was ungauged. Therefore, in an additional experiment, a synthetic stream gauge (S1) was added in the unobserved area for evaluating the effect of the additional observations on the parameter estimation.

### 3.5. Analysis of simulation results

To evaluate the results of the parameter estimation the percentage error and the coefficient of variation (CV) of the estimated Manning's coefficients were determined. It was generally expected that $n$ estimates improve with time, which allowed considering the $n$ values at the end of the time series as best estimates. In order to avoid instantaneous, none-representative values in case of a fluctuating $n$ parameter, not only the very last time steps but the mean of the last 24 update steps was considered as final estimate.

For every stochastic realization the mean $n$ value of the last 24 update steps was computed and these values were averaged over the complete ensemble to calculate the logarithmic mean. This estimated Manning's value $n_{\text{est\_mean}}$ was compared to the reference $n$ value and the percentage error was calculated:

$$n_{\text{est\_mean}} = \exp\left(\frac{1}{64}\sum_{i=1}^{N}\log\left(\frac{1}{24}\sum_{t=nts-23}^{nts} n_{\text{est}}(t,i)\right)\right) \tag{4}$$

$$error(\%) = \left(\frac{n_{\text{est\_mean}}}{n_{\text{ref}}} - 1\right) \times 100 \tag{5}$$

with $n_{\text{est}}(t,i)$ being the estimated Manning's coefficient at update step $t$ and realization $i$, $nts$ being the total number of update steps and $n_{\text{ref}}$ the reference Manning's coefficient.

The ensemble spread is evaluated with the coefficient of variation, being the ratio of the standard deviation and the mean of the distribution:

$$CV(t) = \frac{\sigma(n_{\text{est}}(t))}{\mu(n_{\text{est}}(t))} \tag{6}$$

$$CV_{\text{last24}} = \frac{1}{24}\sum_{t=nts-23}^{t=nts} CV(t) \tag{7}$$

The $CV$ is used instead of the standard deviation or variance because it allows comparing the ensemble spread of the different parameter zones with different Manning's $n$. Again, the mean of the coefficients of variation of the last 24 update steps is considered as the final $CV$.

## 4. Results and discussion

In SA and SB, estimated Manning's coefficients are accurate and precise for the zones forest, field, hillslopes and streams in all cases with spatially distributed precipitation forcing (c1, c2 and c3). Errors in estimated $n$ for these zones range from −5 to 16%. The percentage errors and coefficients of variation of the final estimates are summarized in Table 3 and Table 4. The Manning's coefficient for the streams is estimated most accurately (the error is always less than 1%), because all water level observations are monitored

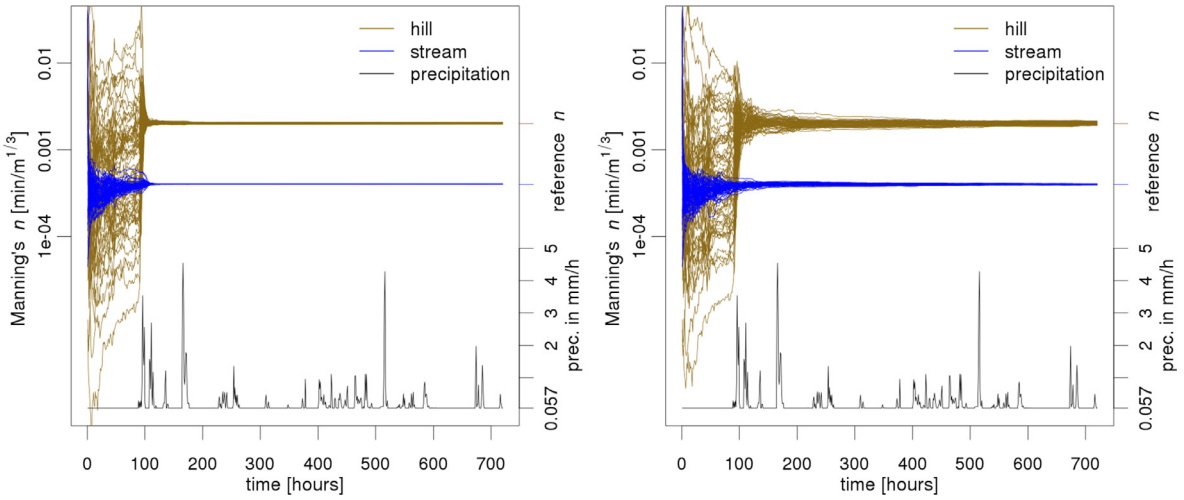


**Fig. 3.** Updated Manning's coefficients with time for scenario A, (left) case 1: error-free precipitation and an absolute observation error; and (right) case 3: perturbed precipitation and a variable observation error. The catchment average precipitation intensity is shown at the bottom.

**Table 3**
Percentage error of estimated Manning's coefficients.

| Runname | Forest | Field/Hill- slopes | Urban | Streams |
|---|---|---|---|---|
| With absolute observation error and error-free precipitation | | | | |
| SA-c1 | | 0.90 | | 0.22 |
| SB1-c1 | 0.57 | 1.24 | 108.16 | 0.03 |
| SB1-c1+S1 | −0.37 | 4.33 | 11.42 | −0.05 |
| SB2-c1 | 1.42 | 1.63 | 91.02 | 0.04 |
| With variable observation error and error-free precipitation | | | | |
| SA-c2 | | 3.83 | | 0.98 |
| SB1-c2 | −0.51 | 0.18 | 357.36 | −0.32 |
| SB1-c2+S1 | −2.83 | 10.61 | 45.02 | −0.47 |
| SB2-c2 | 0.77 | 3.66 | 345.02 | −0.41 |
| With variable observation error and perturbed precipitation | | | | |
| SA-c3 | | 3.25 | | 0.84 |
| SB1-c3 | −3.78 | 6.33 | 381.62 | −0.45 |
| SB1-c3+S1 | −5.18 | 15.95 | 105.31 | −0.81 |
| SB2-c3 | −5.13 | 8.94 | 711.99 | −0.72 |
| With variable observation error, spatially homogeneous perturbed precipitation | | | | |
| SB1-c4 | 37.23 | −6.48 | 146.12 | −4.14 |
| SB2-c4 | 36.01 | −8.77 | 1067.44 | −5.53 |

**Table 4**
Coefficient of variation (x $10^{-2}$) of the ensemble of estimated Manning's coefficients.

| Runname | Forest | Field/Hill-slopes | Urban | Streams |
|---|---|---|---|---|
| With absolute observation error and error-free precipitation | | | | |
| SA-c1 | | 0.89 | | 0.21 |
| SB1-c1 | 2.57 | 2.48 | 41.30 | 0.21 |
| SB1-c1+S1 | 2.56 | 1.90 | 13.04 | 0.21 |
| SB2-c1 | 2.70 | 2.22 | 42.46 | 0.21 |
| With variable observation error and error-free precipitation | | | | |
| SA-c2 | | 3.82 | | 0.98 |
| SB1-c2 | 9.27 | 9.77 | 78.64 | 0.92 |
| SB1-c2+S1 | 8.20 | 7.80 | 39.70 | 0.87 |
| SB2-c2 | 9.15 | 8.73 | 103.25 | 0.97 |
| With variable observation error and perturbed precipitation | | | | |
| SA-c3 | | 3.25 | | 0.84 |
| SB1-c3 | 7.38 | 8.63 | 38.34 | 0.72 |
| SB1-c3+S1 | 5.51 | 7.77 | 20.60 | 0.72 |
| SB2-c3 | 8.07 | 7.09 | 67.42 | 1.02 |
| With variable obs. error, spatially homogeneous perturbed precipitation | | | | |
| SB1-c4 | 7.48 | 9.02 | 43.00 | 1.04 |
| SB2-c4 | 7.55 | 10.81 | 129.45 | 1.30 |

directly in the streams. Also, the two parameters of SA are estimated more accurately than for SB, which has four different parameter values. The results of scenarios B1, B1+S1 and B2, the latter having a lager initial ensemble spread, are very similar in all three cases. Errors in estimated $n$ are only slightly larger for SB2.

For the first three and a half days of the simulation period there was no precipitation, except the temporally and spatially homogeneous background flux. The system was in steady state, temporal changes in water level in the simulations are only introduced by the data assimilation and not by precipitation variations. Temporal variability in stream water level, induced by temporal variable precipitation, is needed to be able to invert upstream parameters. Therefore, before the beginning of distributed precipitation, hardly any information on upstream parameters of the zones hillslopes, field, forest and urban areas could be inverted. On the other hand, the information gained by the synthetic observations in this period was enough to allow for an update of the streams' Manning's coefficient. This was much more straightforward than for the other zones because all observation gauges are located in the streams. The parameter ensemble converges towards the reference value even before the start of distributed precipitation. With the start of precipitation at update step 89, the Manning's $n$ ensembles for hillslopes, field and forest rapidly converged towards the reference value. The temporal evolution of updated $n$ is shown in Fig. 3 for SA-c1 SA-c3 and in Fig. 4 for SB1-c1, SB1-c2 and SB1-c3.

Parameter estimation results of the urban zone are not accurate. The major part of the urban zone is located in the unobserved northeast of the modelling domain and outside of the actual Upper Erft and Swist watersheds. Inside the actual catchment there are only small, distributed patches of urban areas. The parameter update was completely based on these small areas and therefore more difficult than the estimation of $n$ for the streams, field or forest. Though for c1 an improvement in the estimate of the urban zone's $n$ compared to the initial guess with an offset of about factor 3 (300%) to the reference value can be observed, for c2 and c3 there is no improvement in the $n$ estimate compared to the initial guess. Adding an additional stream gauge in the north eastern area significantly improves the parameter estimation in all cases, though the final estimation error is still substantially larger than for the other zones which are better observed. This case demonstrates the usefulness of numerical experiments in monitoring network design.

*Impact of relative observation error*

Applying a relative but larger observation error, the spread in the estimated parameters increased considerably. The increased observation error of c2 compared to c1 reflects a larger uncertainty of the observations, which results in a smaller Kalman gain and therefore a smaller parameter update. The coefficients of variation of the updated parameter for c2 are larger than for c1 by a factor of three to four for all four experiments. Nevertheless, the final $n$ estimates after the 30-days assimilation period exhibit about the same accuracy as with the smaller, absolute observation error.

*Impact of rain radar error*

Perturbed precipitation fields were applied to account for measurement uncertainty in radar precipitation data. For SA with only two parameters the estimation of the Manning's $n$ for case 3 (perturbed precipitation) is as accurate as for case 2 (error-free precipitation) (both with a large, variable observation error). For SB with four parameter zones the estimated $n$ parameters are slightly less accurate in the case of perturbed precipitation, but still good (compare Table 3). The percentage error of the estimated parameters is about 3–5% larger if perturbed precipitation is applied (compared to error free precipitation). The final ensemble spread of $n$ is slightly smaller if perturbed precipitation was applied, compared to the case of error free precipitation. The coefficient of variation for the last 24 time steps is 10–20% smaller for all experiments of case 3 compared to case 2 (compare Table 4). Considering the additional uncertainty introduced by the perturbation of the precipitation data, one could expect a larger ensemble spread. As shown in Fig. 5 the ensemble spread, here expressed as the ensemble variance, does initially decrease more slowly if precipitation is perturbed, for all experiments. Once the parameter ensemble spread is already low, the ensemble converges stronger in the case of perturbed precipitation resulting in a lower ensemble spread at the end of the assimilation time series. For the urban zone the ensemble spread clearly underestimates the uncertainty in the parameter estimate, because in the case of perturbed precipitation the ensemble of $n_{\text{urban}}$does not cover the reference value. Possibly, the low ensemble spread of the other zones' $n$ underestimates the uncertainty, too.

In a fourth case (c4), the realizations were forced with spatially averaged, homogeneous precipitation data to assess the importance of realistic, spatially distributed precipitation forcing for the parameter estimation. The final errors of $n$ estimates are larger than with spatially distributed precipitation (case 3) by a factor of about 10 for the zones forest and streams. Still, $n$ estimates for streams are reasonable, and the accuracy of the field-zone $n$ is as good as with distributed precipitation. One reason may be the large spatial extensions of the zones, which mitigate the need for spatially distributed precipitation. Furthermore, the joint state-parameter update decreases the offset in water levels caused by the inaccurate precipitation forcing. Consequently, the offset in water level does not accumulate in time and facilitates the parameter estimation. Nevertheless, the results show that realistic, spatially distributed precipitation forcing is of advantage for the catchment tomography approach.

Note, additionally to the discussed experiments, the concept was tested on a fully distributed Manning's field with spatially correlated $n$. This scenario was implemented with the variable observation error and perturbed precipitation. Though a clear improvement in Manning's estimates (compared to the initial guess) could be observed, the results are not yet satisfactory. The ensemble converged very fast to one Manning's field, which resembles the reference field but significant differences remained. Filter inbreeding inhibited the information potential of new observations. This suggests that more complex scenarios require considerably larger ensemble sizes to handle filter inbreeding and sampling uncertainty, which can (at least partly) be mitigated by damping and covariance inflation.

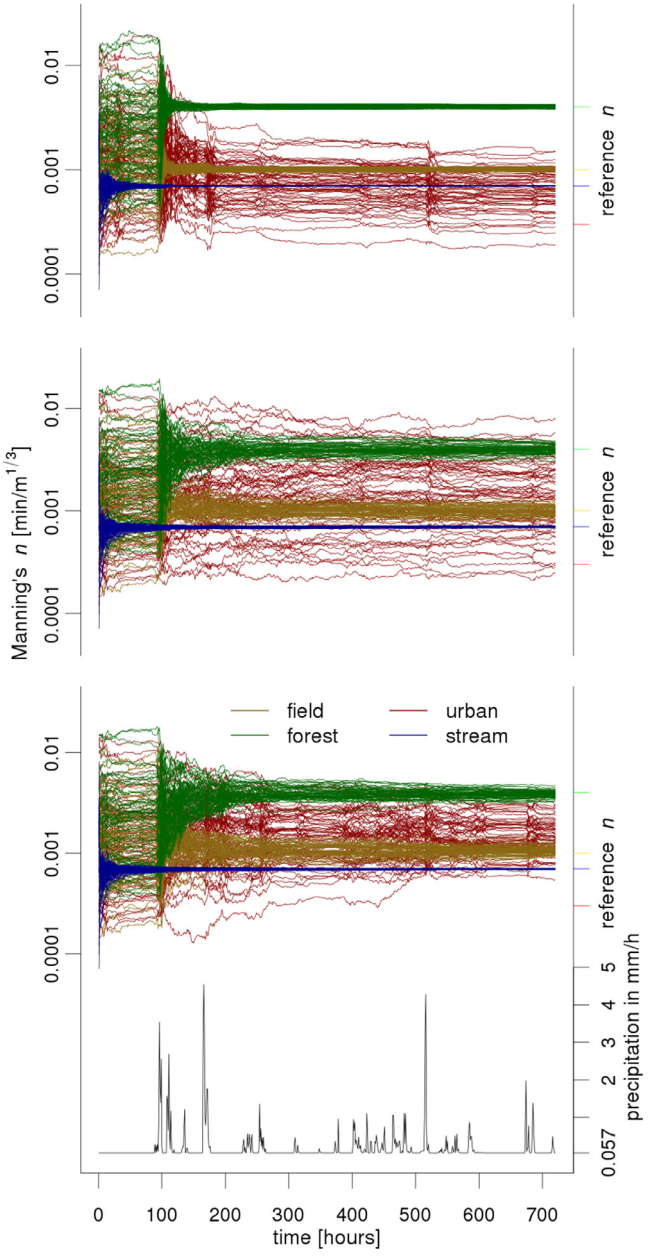


**Fig. 4.** Estimated Manning's coefficients with time for scenario B1, (top) case 1: error-free precipitation and an absolute observation error, (middle) error-free precipitation and variable observation error and (bottom) case 3: perturbed precipitation and a variable observation error. The catchment average precipitation intensity is shown at the bottom.

These results show that the estimation of a spatially distributed Manning's $n$ by assimilating water level observations into a hydrological model is efficient if highly distributed precipitation forcing is applied. During the major part of the 30-days modelling and assimilation period there was hardly any change on the updated parameters (compare Fig. 3 and Fig. 4), which means that shorter time series would have been similarly efficient. More important than the length of the assimilation time series is the occurrence of precipitation, which is demonstrated by the strong ensemble convergence with precipitation events. A strong increase in

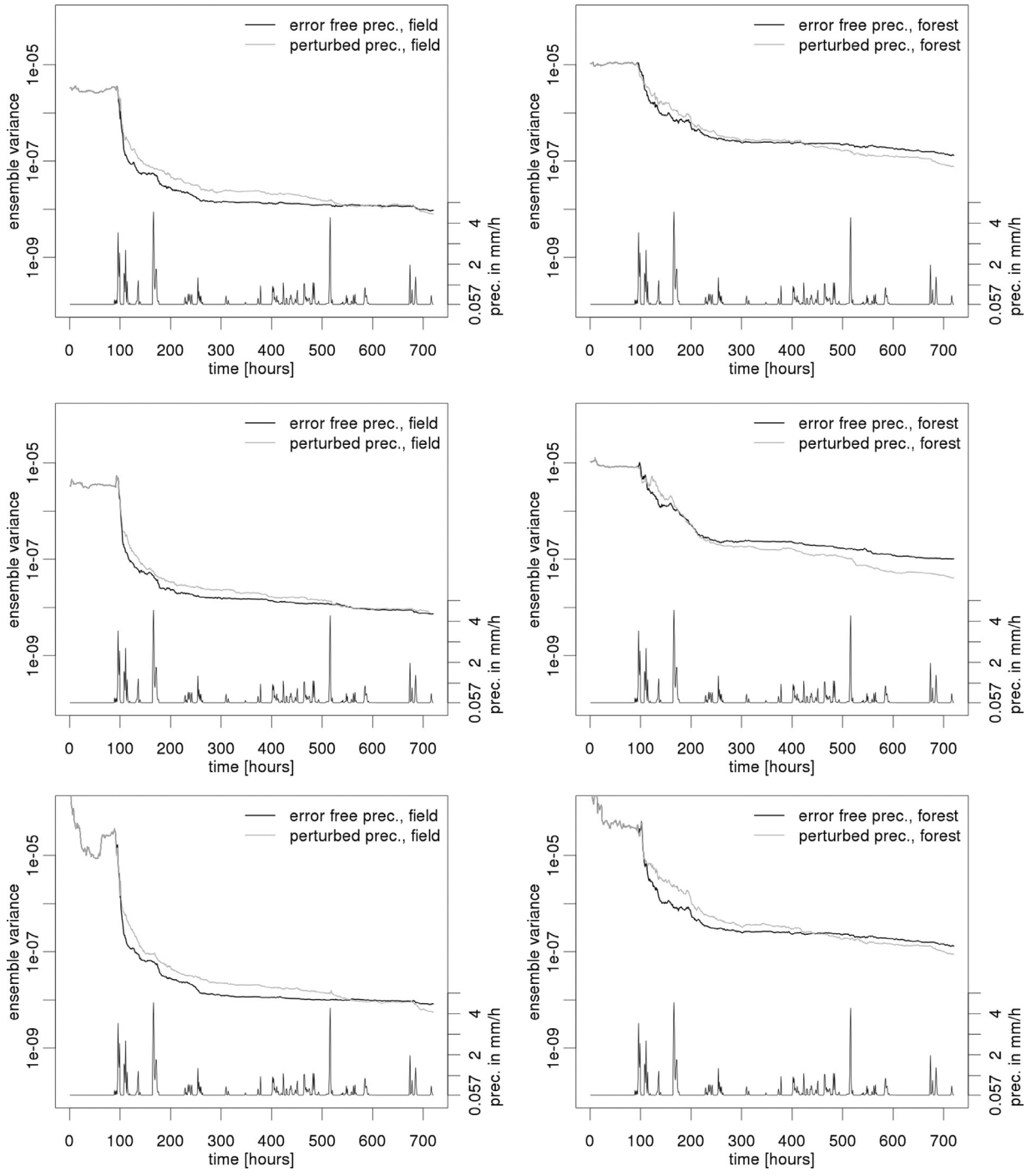


**Fig. 5.** Ensemble variance of Manning's $n$ for error-free and perturbed precipitation forcing, (left) field and (right) forest, (top) SB1, (middle) SB1+S1, (bottom) SB2.

the observation error did not alter the parameter estimation accuracy and the larger uncertainty was realistically represented by a larger ensemble spread. This shows that the approach is robust in case of unbiased observation errors. In case of precipitation errors, increased uncertainty resulted in a slightly smaller ensemble spread. The issue of ensemble convergence or filter inbreeding for parameters estimated by data assimilation was already discussed by Franssen and Kinzelbach (2008). Though it did not result in a problem in this study as the parameter estimates were still good, it is important to be aware that the ensemble spread of parameters estimated by a joint state-parameter estimation may not realistically reflect the parameter uncertainty.

For further developing the catchment tomography approach for distributed parameter estimation with physically based rainfall-runoff models, methods for maintaining the parameter ensemble spread will be beneficial. Further synthetic studies will be needed for advancing this approach towards a real world application. Currently catchment tomography is a novel, CPU intensive approach, where synthetic experiments are valuable for testing different assimilation methods, methods to handle filter inbreeding and network design. The integration of a subsurface into the model will evoke several more research questions. A lower sensitivity of stream water level to the Manning's coefficient may challenge this approach and raise the need for longer assimilation periods. Fur-

thermore, subsurface parameters will add additional uncertainty to the parameter estimation. The time lag between precipitation events and the resulting changes in observed stream water level will be larger once subsurface flow will be modeled. Thus, an ensemble Kalman smoother is expected to perform better than a filter. These innovations will need further synthetic research before applying this CPU-intensive method to real-world problems.

## 5. Summary and conclusions

A catchment tomography approach was applied in synthetic experiments to estimate the spatially distributed Manning's roughness coefficient. A 2D catchment model simulating overland flow was forced with high resolution radar precipitation data. Forward simulations were performed with the hydrologic model ParFlow, which has been coupled to the Parallel Data Assimilation Framework (PDAF) for data assimilation. Precipitation served as transmitter in this tomographic approach, generating runoff along different paths and resulting in an integrated signal in the form of frequent stream water level measurements. These measurements collected at synthetic gauges resembling the receivers, were assimilated into a hydrological model. By a joint state-parameter update with the Ensemble Kalman Filter these measurements were inverted to estimate the Manning's roughness coefficient. The uncertain Manning $n$ coefficient was continuously constrained by sequentially integrating new information.

The proposed catchment tomography approach successfully estimated the spatial distribution of Manning's coefficient with only 64 realizations. The parameter estimation became very effective as soon as there was spatially and temporally distributed precipitation. Only for an area located mostly outside of the gauged catchment the estimation of $n$ was prone with large uncertainties because of missing observations. Adding an additional observation gauge in this area reduced the uncertainty and provided better estimates of the Manning's coefficient. The approach is applicable to any catchment where stream flow is sensitive to the parameters to be estimated and high quality data of distributed precipitation, topography and stream water level observations are available.

Experiments were performed with a spatio-temporally constant absolute observation error and with a more realistic relative, and also larger, observation error. Results showed that there was no increase in estimation error applying the larger relative observation error, but the remaining parameter uncertainty was better represented by a larger ensemble spread of estimated $n$. When applying perturbed precipitation fields the ensemble of estimated $n$ converged slightly slower than with error-free precipitation. Nevertheless, this resulted in an even smaller final ensemble spread, with a coefficient of variation about 10–20% smaller as for the case with error-free precipitation. Though estimation results had larger errors by 3–5% for the zones field and forest and 0.3% for the zone streams with perturbed than error-free precipitation forcing, overall the impact of perturbed precipitation on the parameter estimation was very limited. Nevertheless the application of perturbed precipitation is important to account for the uncertainty in radar precipitation estimates, while this type of uncertainty does not appear to significantly limit the efficiency of the suggested catchment tomography approach.

Applying spatially averaged precipitation fields (instead of heterogeneous fields) on the model realizations resulted in a larger estimation error for the zones forest and streams by a factor of ten, while the estimated $n$ for the zone field had the same errors as in the case with spatially distributed precipitation (about 6% and 9% for SB1 and SB2, respectively). While zonation of parameters as applied for the presented experiments reduced the necessity of applying spatially distributed precipitation fields, realistic precipitation forcing resulted in significantly better parameter estimates, which we assume to be even more pronounced for more complex scenarios.

The proposed catchment tomography approach showed overall good experimental results with a strong potential for further research and applications. Using larger ensemble sizes will likely enable the estimation of fully distributed parameter fields. Depending on the future application, methods to reduce filter inbreeding or to account for the time lag between precipitation and water level measurements like a smoother, may be beneficial and will be subject of further research. Thus, catchment tomography based on rain radar information is a promising method for distributed parameter estimation in catchment hydrology and valuable for improved flood prediction.

## Acknowledgements

This research is financed by the SFB-TR32 "Patterns in soil–vegetation–atmosphere systems: monitoring, modelling and data assimilation" funded by the German Science Foundation (DFG). The authors gratefully acknowledge the Erft-Verband for their advice in selecting the sample catchment and for providing stream gauge data. We also would like to thank Malte Diederich (Bonn University) for supplying the radar based precipitation estimates used in this study. We are grateful to two anonymous reviewers, Jasper Vrugt, the associate editor and the editor Paolo D'Odorico for their thoughtful comments and suggestions which considerably improved the quality of this manuscript.

## Appendix: The Ensemble Kalman Filter for joint state and parameter estimation

*The Kalman Filter*

The Kalman Filter is a sequential data assimilation method. A state forecast, usually a model simulation of the desired state, is updated with another estimate of the state or a related state, usually an observation. The updated state vector, the so called analysis, is a linear combination of the forecasted state vector and the observation vector. The Kalman gain $\mathbf{K}$ weights the two estimates (model forecast and observation) according to their variances, minimizing the variance of the resulting state analysis. The Kalman Filter is therefore basically a maximum likelihood estimator.

The state forecast $\mathbf{s}^f$ of dimensions $m \times 1$ contains the modelled states at all $m$ spatial locations of the model grid. The state observation vector $\mathbf{y_s}$ of dimensions $M_s \times 1$ contains all $M_s$ available state observations.

The state analysis vector $\mathbf{s}^a$ is a linear combination of $\mathbf{s}^f$ and $\mathbf{y_s}$:

$$\mathbf{s}^a = \mathbf{s}^f + \mathbf{K}\left(\mathbf{y_s} - \mathbf{H}\mathbf{s}^f\right) \tag{A.1}$$

where $\mathbf{H}$ $(M_s \times m)$ is the observation operator which maps the state vector $\mathbf{s}^f$ on the observation vector $\mathbf{y_s}$. This is necessary because usually there are fewer observations than model grid cells and often the measured state is related to, but not exactly the same as the modeled state. $\mathbf{H}\mathbf{s}^f$ gives a model prediction of the observations which are then compared to the real observations $\mathbf{y_s}$ in the second term of (A.1): $\mathbf{y}_s - \mathbf{H}\mathbf{s}^f$. This difference between real and predicted observations is used to update the model state forecast in the analysis step. The Kalman gain $\mathbf{K}$ weights the uncertainties of model forecast and observations. The less uncertain the observation is compared to the model forecast, the larger is the Kalman gain, and vice versa. The larger the Kalman gain, the larger the correction $\mathbf{K}(\mathbf{y}_s - \mathbf{H}\mathbf{s}^f)$ which is added to the model forecast in the analysis step (Eq. (A.1)).

In a scalar case, with $m=1$ and $M_s=1$ the Kalman gain K is the variance of the model forecast $\sigma_f^2$ divided by the sum of the

variances of the model forecast and the observation $\sigma^2_{obs}$:

$$K = \frac{\sigma_f^2}{\sigma_f^2 + \sigma_{obs}^2} \tag{A.2}$$

In the scalar case the observation location is identical with the update location. In the vector case a distributed, gridded variable is updated with observations at few individual grid cells. The update location is mostly different from the observation location. Therefore, instead of considering a single variance of the state forecast, the Kalman gain is computed from the forecast error covariance matrix $\mathbf{C_{ss}}$ and the observation error covariance matrix $\mathbf{R}$. $\mathbf{C_{ss}}$ contains the covariances of the variable to be updated for all grid cell combinations and has thus dimensions $m \times m$. $\mathbf{R}$ contains the covariances between all observations and is here a diagonal matrix because observations are treated to be uncorrelated.

The Kalman gain is then given by:

$$\mathbf{K} = \mathbf{C_{ss}}\mathbf{H}^{\mathrm{T}}\left(\mathbf{H}\mathbf{C_{ss}}\mathbf{H}^{\mathrm{T}} + \mathbf{R}\right)^{-1} \tag{A.3}$$

*The ensemble Kalman Filter*

Eq. (A.3) demonstrates that the model forecast and observation error covariance matrices need to be known for every update. The ensemble Kalman Filter estimates the model error covariance matrix from an ensemble of possible model states $\mathbf{s}_i^f$ with realizations $i = 1, ..., N$. The ensemble mean of the state forecast $\overline{\mathbf{s}_i^f}$ is assumed to be the best estimate of the true state. Instead of computing the model error covariance matrix from the deviation from the true, but unknown state vector $\mathbf{s}^{true}$:

$$\mathbf{C_{ss}} = \overline{(\mathbf{s}^f - \mathbf{s}^{true})(\mathbf{s}^f - \mathbf{s}^{true})^{\mathrm{T}}} \tag{A.4}$$

The model ensemble covariance matrix $\mathbf{C}^e_{\mathbf{ss}}$ is estimated as:

$$\mathbf{C}^e_{\mathbf{ss}} = \overline{(\mathbf{s}_i^f - \overline{\mathbf{s}^f})(\mathbf{s}_i^f - \overline{\mathbf{s}^f})^{\mathrm{T}}} \tag{A.5}$$

where the overbar expresses the expected value.

The model covariance matrix is approximated by the Ensemble Kalman Filter according:

$$\mathbf{C}^e_{\mathbf{ss}} = \frac{1}{N-1}\sum_{i=1}^{N}\left(\mathbf{s}_i^f - \overline{\mathbf{s}^f}\right)\left(\mathbf{s}_i^f - \overline{\mathbf{s}^f}\right)^{\mathrm{T}} \tag{A.6}$$

The observations need to be perturbed as well to avoid an underestimation of the analysis ensemble covariance, as clarified by Burgers et al. (1998). The ensemble of observations is generated by adding a random perturbation $\boldsymbol{\varepsilon}_i$ with zero mean and a variance equal to the estimated measurement error variance:

$$\mathbf{y}_{\mathbf{s}i} = \mathbf{y}_{\mathbf{s}} + \boldsymbol{\varepsilon}_i \tag{A.7}$$

Where $\mathbf{y}_{\mathbf{s}i}$ is the $i^{th}$ realization of the perturbed observation vector.

Note that the perturbation of observations also causes additional sampling errors and may therefore reduce the accuracy of the filter. For details and alternatives please refer to Whitaker and Hamill (2002) or Tippett et al. (2003)

The ensemble state analysis vector $\mathbf{s}_i^a$ is computed by updating every ensemble member:

$$\mathbf{s}_i^a = \mathbf{s}_i^f + \mathbf{K}\left(\mathbf{y}_{\mathbf{s}i} - \mathbf{H}\mathbf{s}_i^f\right) \tag{A.8}$$

*Joint state-parameter estimating with EnKF*

Model parameters can be updated jointly with model states, with or without observations of the parameter itself. Therefore, the state forecast $\mathbf{s}^f$ is augmented by the parameter vector $\mathbf{p}^f$ to form a joint state-parameter vector $\mathbf{x}_i^f$:

$$\mathbf{x}_i^f = \begin{bmatrix}\mathbf{s}_i^f \\ \mathbf{p}_i^f\end{bmatrix} \tag{A.9}$$

The parameters are here not anymore considered to be invariable in time but are updated in the analysis step, just like the states. To apply this state augmentation approach with the EnKF, an ensemble of parameter samples, ideally representing the uncertainty of the parameter estimates, needs to be generated.

If there are observations of the parameter available, the state observation vector is augmented to a state-parameter observation vector:

$$\mathbf{y}_{\mathbf{x}i} = \begin{bmatrix}\mathbf{y}_{\mathbf{s}i} \\ \mathbf{y}_{\mathbf{p}i}\end{bmatrix} \tag{A.10}$$

of dimension $M_s + M_p$. $M_p$ is the number of observed parameters. The total number of observations is $M_x = M_s + M_p$.

The model covariance matrix includes now states and parameters. It is computed from the ensemble of joint state-parameter vectors and is given by:

$$\mathbf{C}^e_{\mathbf{xx}} = \begin{bmatrix}\mathbf{C}^e_{\mathbf{ss}} & \mathbf{C}^e_{\mathbf{sp}} \\ \mathbf{C}^e_{\mathbf{ps}} & \mathbf{C}^e_{\mathbf{pp}}\end{bmatrix} \tag{A.11}$$

Note that in the case presented in this study there are no observations of the parameter available so that $M_p = 0$ and $\mathbf{y}_{\mathbf{p}i} = 0$. The parameters are solely updated with state observations. Parameters will only be updated if the covariance between states and parameters differs from zero. If state and parameter observations were available, both states and parameters could be updated by state and parameter observations.

The augmented Kalman gain $\mathbf{K_x}$ is computed now as follows:

$$\mathbf{K_x} = \mathbf{C}^{\mathbf{e}}_{\mathbf{xx}}\mathbf{H}^{\mathbf{T}}_{\mathbf{x}}\left(\mathbf{H_x}\mathbf{C}^{\mathbf{e}}_{\mathbf{xx}}\mathbf{H}^{\mathrm{T}}_{\mathbf{x}} + \mathbf{R_x}\right)^{-1} \tag{A.12}$$

and has dimensions $2m \times M_x$. The observation error covariance matrix $\mathbf{R_x}$ has dimensions $M_x \times M_x$.

The analyzed joint state-parameter vector $\mathbf{x}_i^a$ is computed as follows:

$$\mathbf{x}_i^a = \mathbf{x}_i^f + \mathbf{K_x}\left(\mathbf{y}_{\mathbf{x}i} - \mathbf{H_x}\mathbf{x}_i^f\right) \tag{A.13}$$

In this study the updated parameters contained in the vector $\mathbf{p}$ are logarithmic transformed Manning's coefficients. The covariances and Kalman gain are calculated on the basis of logarithmic transformed Manningś coefficients.

## References


Anderson, J.L., 2001. An ensemble adjustment Kalman filter for data assimilation. Mon. Weather Rev. 129, 2884–2903.

Annan, J.D., Hargreaves, J.C., Edwards, N.R., Marsh, R., 2005. Parameter estimation in an intermediate complexity earth system model using an ensemble Kalman filter. Ocean Modell. 8, 135–154.

Arcement, G.J., Schneider, V.R., 1989. Guide for Selecting Manning's Roughenss Coefficients for Natural Channels And Flood Plains. US Geological Survey, p. 2339.

Ashby, S.F., Falgout, R.D., 1996. A parallel multigrid preconditioned conjugate gradient algorithm for groundwater flow simulations. Nucl. Sci. Eng. 124, 145–159.

Bailey, R.T., Bau, D., 2012. Estimating geostatistical parameters and spatially-variable hydraulic conductivity within a catchment system using an ensemble smoother. Hydrol. Earth Syst. Sci. 16, 287–304.

Baldauf, M., Seifert, A., Forstner, J., Majewski, D., Raschendorfer, M., Reinhardt, T., 2011. Operational convective-scale numerical weather prediction with the COSMO model: description and sensitivities. Mon. Weather Rev. 139, 3887–3905.

Bishop, C.H., Etherton, B.J., Majumdar, S.J., 2001. Adaptive sampling with the ensemble transform Kalman filter. Part I: Theoretical aspects. Mon. Weather Review 129, 420–436.

Bourdin, D.R., Fleming, S.W., Stull, R.B., 2012. Streamflow modelling: A primer on applications, approaches and challenges. Atmos. Ocean 50, 507–536.

Burgers, G., van Leeuwen, P.J., Evensen, G., 1998. Analysis scheme in the ensemble Kalman filter. Mon. Weather Review 126, 1719–1724.

Camporese, M., Paniconi, C., Putti, M., Salandin, P., 2009a. Comparison of data assimilation techniques for a coupled model of surface and subsurface flow. Vadose Zone J. 8, 837–845.

Camporese, M., Paniconi, C., Putti, M., Salandin, P., 2009b. Ensemble Kalman filter data assimilation for a process-based catchment scale model of surface and subsurface flow. Water Resour. Res. 45.

Chen, Y., Zhang, D.X., 2006. Data assimilation for transient flow in geologic formations via ensemble Kalman filter. Adv. Water Res. 29, 1107–1122.

Chow, V.-T., Mays, L.W., Maidment, D.R., 1988. Applied Hydrology. McGraw-Hill, New York.
Clark, M.P., Rupp, D.E., Woods, R.A., Zheng, X., Ibbitt, R.P., Slater, A.G., Schmidt, J., Uddstrom, M.J., 2008. Hydrological data assimilation with the ensemble Kalman filter: Use of streamflow observations to update states in a distributed hydrological model. Adv. Water Res. 31, 1309–1324.
Di Baldassarre, G., Montanari, A., 2009. Uncertainty in river discharge observations: a quantitative analysis. Hydrol. Earth Syst. Sci. 13, 913–921.
Diederich, M., Ryzhkov, A., Simmer, C., Zhang, P.F., Tromel, S., 2015a. Use of specific attenuation for rainfall measurement at x-band radar wavelengths. part I: radar calibration and partial beam blockage estimation. J. Hydrometeorology 16, 487–502.
Diederich, M., Ryzhkov, A., Simmer, C., Zhang, P.F., Tromel, S., 2015b. Use of specific attenuation for rainfall measurement at x-band radar wavelengths. part II: rainfall estimates and comparison with rain gauges. J. Hydrometeorology 16, 503–516.
Ehrendorfer, M., 2007. A review of issues in ensemble-based Kalman filtering. Meteorol. Z. 16, 795–818.
Evensen, G., 1994. Sequential data assimilation with a nonlinear quasi-geostrophic model using monte-carlo methods to forecast error statistics. J. Geophys. Res.-Oceans 99, 10143–10162.
Evensen, G., van Leeuwen, P.J., 2000. An ensemble Kalman smoother for nonlinear dynamics. Mon. Weather Review 128, 1852–1867.
Franssen, H.J.H., Kinzelbach, W., 2008. Real-time groundwater flow modeling with the Ensemble Kalman Filter: Joint estimation of states and parameters and the filter inbreeding problem. Water Resour. Res. 44.
Houtekamer, P.L., Mitchell, H.L., 1998. Data assimilation using an ensemble Kalman filter technique. Mon. Weather Rev. 126, 796–811.
Jones, J.E., Woodward, C.S., 2001. Newton–Krylov-multigrid solvers for large-scale, highly heterogeneous, variably saturated flow problems. Adv. Water Res. 24, 763–774.
Kalman, R.E., 1960. A new approach to linear filtering and prediction problems. J. Basic Eng. 82 (1), 35–45.
Karnahl, J.A., 2008. 2D numerische Modellierung von multifraktionalem Schwestoff- und Schadstofftransport in Flüssen. Eigenverlag des Instituts für Wasserbau der Universität Stuttgart 177.
Kitanidis, P.K., Bras, R.L., 1980a. Real-Time Forecasting with a Conceptual Hydrologic Model 0.1. Analysis of Uncertainty. Water Resour. Res. 16, 1025–1033.
Kitanidis, P.K., Bras, R.L., 1980b. Real-Time Forecasting with a Conceptual Hydrologic Model 0.2. Applications and Results. Water Resour. Res. 16, 1034–1044.
Kollet, S.J., Maxwell, R.M., 2006. Integrated surface-groundwater flow modeling: A free-surface overland flow boundary condition in a parallel groundwater flow model. Adv. Water Res. 29, 945–958.
Kollet, S.J., Maxwell, R.M., Woodward, C.S., Smith, S., Vanderborght, J., Vereecken, H., Simmer, C., 2010. Proof of concept of regional scale hydrologic simulations at hydrologic resolution utilizing massively parallel computer resources. Water Resour. Res. 46.
Kurtz, W., Franssen, H.J.H., Vereecken, H., 2012. Identification of time-variant river bed properties with the ensemble Kalman filter. Water Resour. Res. 48.
Kurtz, W., HE, G., Kollet, S.J., Maxwell, R.M., Vereecken, H., Franssen, Hendricks, H., J., 2016. TerrSysMP–PDAF (version 1.0): a modular high-performance data assimilation framework for an integrated land surface–subsurface model. Geosci. Model Dev. 9, 1341–1360.
Li, W., Englert, A., Cirpka, O.A., Vanderborght, J., Vereecken, H., 2007. Two-dimensional characterization of hydraulic heterogeneity by multiple pumping tests. Water Resour. Res. 43.
Liu, Y., Weerts, A.H., Clark, M., Franssen, H.J.H., Kumar, S., Moradkhani, H., Seo, D.J., Schwanenberg, D., Smith, P., Van Dijk, A.I.J.M., Van Velzen, N., He, M., Lee, H., Noh, S.J., Rakovec, O., Restrepo, P., 2012. Advancing data assimilation in operational hydrologic forecasting: progresses, challenges, and emerging opportunities. Hydrol. Earth Syst. Sci. 16, 3863–3887.
Madsen, H., Rosbjerg, D., Damgard, J., Hansen, F.S., 2003. Data assimilation in the MIKE 11 flood forecasting system using Kalman filtering. In: Water Resources Systems-Hydrological Risk, Management and Development, pp. 75–81.
Maxwell, R.M., Condon, L.E., Kollet, S.J., 2015. A high-resolution simulation of groundwater and surface water over most of the continental US with the integrated hydrologic model ParFlow v3. Geosci. Model Dev. 8, 923–937.
Maxwell, R.M., Kollet, S.J., Smith, S.G., Woodward, C.S., Falgout, R.D., Ferguson, I.M., Baldwin, C., Bosl, W.J., Hornung, R., Ashby, S., 2010. ParFlow User's Manual. International Ground Water Modeling Center 132 Report GWMI 2010-01.
Mclaughlin, D., 2002. An integrated approach to hydrologic data assimilation: interpolation, smoothing, and filtering. Adv. Water Res. 25, 1275–1286.
Mcmillan, H.K., Hreinsson, E.O., Clark, M.P., Singh, S.K., Zammit, C., Uddstrom, M.J., 2013. Operational hydrological data assimilation with the recursive ensemble Kalman filter. Hydrol. Earth Syst. Sci. 17, 21–38.
Montzka, C., Pauwels, V.R.N., Franssen, H.J.H., Han, X.J., Vereecken, H., 2012. Multivariate and Multiscale Data Assimilation in Terrestrial Systems: A Review. Sensors 12, 16291–16333.
Moradkhani, H., Sorooshian, S., Gupta, H.V., Houser, P.R., 2005. Dual state-parameter estimation of hydrological models using ensemble Kalman filter. Adv. Water Res. 28, 135–147.
Nerger, L., Hiller, W., 2013. Software for ensemble-based data assimilation systems-Implementation strategies and scalability. Comput. Geosci. 55, 110–118.
Nerger, L., Hiller, W., Schroter, J., 2005. PDAF - The parallel data assimilation framework: Experiences with Kalman filtering. Use of High Performance Computing in Meteorology 63–83.
Oleson, K.W., Niu, G.Y., Yang, Z.L., Lawrence, D.M., Thornton, P.E., Lawrence, P.J., Stockli, R., Dickinson, R.E., Bonan, G.B., Levis, S., Dai, A., Qian, T., 2008. Improvements to the Community Land Model and their impact on the hydrological cycle. J. Geophys. Res.-Biogeosci. 113.
Paiva, R.C.D., Collischonn, W., Bonnet, M.P., De Goncalves, L.G.G., Calmant, S., Getirana, A., Da Silva, J.S., 2013. Assimilating in situ and radar altimetry data into a large-scale hydrologic-hydrodynamic model for streamflow forecast in the Amazon. Hydrol. Earth Syst. Sci. 17, 2929–2946.
Pasche, E., Kräßig, S., Lippert, K., Nasermoaddeli, H., Plöger, W., Rath, S., 2006. Wie viel Physik braucht die Strömungsberechnung in der Ingenieurpraxis. Dresdner wasserbauliche Mitteilungen 32.
Pathiraja, S., Marshall, L., Sharma, A., Moradkhani, H., 2016. Detecting non-stationary hydrologic model parameters in a paired catchment system using data assimilation. Adv. Water Res. 94, 103–119.
Pauwels, V.R.N., De Lannoy, G.J.M., 2006. Improvement of modeled soil wetness conditions and turbulent fluxes through the assimilation of observed discharge. J. Hydrometeorology 7, 458–477.
Pauwels, V.R.N., De Lannoy, G.J.M., 2009. Ensemble-based assimilation of discharge into rainfall-runoff models: A comparison of approaches to mapping observational information to state space. Water Resour. Res. 45.
Pebesma, E.J., 2004. Multivariable geostatistics in S: the gstat package. Computers Geosci. 30, 683–691.
Pokhrel, P., Gupta, H.V., 2011. On the ability to infer spatial catchment variability using streamflow hydrographs. Water Resour. Res. 47.
R Development Core Team, 2008. R: A language and Environment For Statistical Computing. R Foundation for Statistical Computing, Vienna, Austria ISBN 3-900051-07-0URL http://www.R-project.org.
Rakovec, O., Weerts, A.H., Hazenberg, P., Torfs, P.J.J.F., Uijlenhoet, R., 2012. State updating of a distributed hydrological model with Ensemble Kalman Filtering: effects of updating frequency and observation network density on forecast accuracy. Hydrol. Earth Syst. Sci. 16, 3435–3449.
Rakovec, O., Weerts, A.H., Sumihar, J., Uijlenhoet, R., 2015. Operational aspects of asynchronous filtering for flood forecasting. Hydrol. Earth Syst. Sci. 19, 2911–2924.
Rasmussen, J., Madsen, H., Jensen, K.H., Refsgaard, J.C., 2015. Data assimilation in integrated hydrological modeling using ensemble Kalman filtering: evaluating the effect of ensemble size and localization on filter performance. Hydrol. Earth Syst. Sci. Discuss. 12, 2267–2304.
Reichle, R.H., 2008. Data assimilation methods in the Earth sciences. Adv. Water Res. 31, 1411–1418.
Reichle, R.H., Mclaughlin, D.B., Entekhabi, D., 2002a. Hydrologic data assimilation with the ensemble Kalman filter. Mon. Weather Review 130, 103–114.
Reichle, R.H., Walker, J.P., Koster, R.D., Houser, P.R., 2002b. Extended versus ensemble Kalman filtering for land data assimilation. J. Hydrometeorology 3, 728–740.
Sakov, P., Evensen, G., Bertino, L., 2010. Asynchronous data assimilation with the EnKF. Tellus Series a-Dynamic Meteorology and Oceanography 62, 24–29.
Shi, Y.N., Davis, K.J., Zhang, F.Q., Duffy, C.J., Yu, X., 2014. Parameter estimation of a physically based land surface hydrologic model using the ensemble Kalman filter: A synthetic experiment. Water Resour. Res. 50, 706–724.
Shrestha, P., Sulis, M., Masbou, M., Kollet, S., Simmer, C., 2014. A Scale-Consistent Terrestrial Systems Modeling Platform Based on COSMO, CLM, and ParFlow. Mon. Weather Review 142, 3466–3483.
Tippett, M.K., Anderson, J.L., Bishop, C.H., Hamill, T.M., Whitaker, J.S., 2003. Ensemble square root filters. Mon. Weather Review 131, 1485–1490.
Valcke, S., 2013. The OASIS3 coupler: a European climate modelling community software. Geosci. Model Dev. 6, 373–388.
van Leeuwen, P.J., 1999. Comment on "Data assimilation using an ensemble Kalman filter technique". Mon. Weather Review 127, 1374–1377.
Vrugt, J.A., Diks, C.G.H., Gupta, H.V., Bouten, W., Verstraten, J.M., 2005. Improved treatment of uncertainty in hydrologic modeling: Combining the strengths of global optimization and data assimilation. Water Resour. Res. 41.
Vrugt, J.A., Gupta, H.V., Nuallain, B.O., 2006. Real-time data assimilation for operational ensemble streamflow forecasting. J. Hydrometeorology 7, 548–565.
Whitaker, J.S., Hamill, T.M., 2002. Ensemble data assimilation without perturbed observations. Mon. Weather Review 130, 1913–1924.
Yeh, T.C.J., Liu, S.Y., 2000. Hydraulic tomography: Development of a new aquifer test method. Water Resour. Res. 36, 2095–2105.
Yeh, W.W.G., 1986. Review of Parameter-Identification Procedures in Groundwater Hydrology - the Inverse Problem. Water Resour. Res. 22, 95–108.